Thermal Diffusivity of Sintered 12CaO·7Al$_2$O$_3$

P. M. Nikolić[1*], D. Luković[1], S. Savić[1], D. Urošević[2], S. Djurić[1]
[1] Institute of Technical Sciences of SASA, Knez-Mihailova 35/IV, 11000 Belgrade, Serbia
[2] Mathematical Institute of SASA, Knez-Mihailova 35/I, 11000 Belgrade, Serbia

Abstract: *The thermal diffusivity and some electrical transport properties of sintered 12CaO·7Al$_2$O$_3$ were determined using a photoacoustic method with a transmission detection configuration. The thermal diffusivity, coefficient of carrier diffusion and the surface recombination velocities were determined by fitting experimental spectra and theoretical photoacoustic amplitude and phase signals.*
Keywords: *Sintering; Photoacoustic Measurement; Thermal Diffusivity; 12CaO·7Al$_2$O$_3$.*

Резюме: *Для определения температуропроводности и некоторых электрических транспортных свойств спеченного 12CaO·7Al$_2$O$_3$ использован фотоакустический метод. Температуропроводность, коэффициент диффузии свободных носителей, а также скорость поверхностной рекомбинации определены методом приведения в соответствие экспериментальных фотоакустических амплитудных и фазовых сигналов.*
Ключевые слова: *Спекание; фотоакустический метод; температуропроводность, 12CaO·7Al$_2$O$_3$.*

Садржај: *Топлотна дифизивност и нека електрична својства синтерованог 12CaO·7Al$_2$O$_3$ одређивани су коришћењем фотоакустичке методе са трансмисионом детекционом конфигурацијом. Топлотна дифузивност, коефицијент дифузије слободних носилаца, као и брзина површинске рекомбинације одређени су поступком фитовања експерименталних фотоакустичких амплитудских и фазних сигнала.*
Кључне речи: *Синтеровање; фотоакустична метода; топлотна дифузивност; 12CaO·7Al$_2$O$_3$.*

1. Introduction

Increased attention has been paid recently to the insulating oxide 12CaO·7Al$_2$O$_3$ (*C12A7*) because it can be used for obtaining high purity O$^-$ negative ion emission [1] at its surface temperature of only 800ºC and extraction field over 1000 V/cm.

The unit cell (I43d) with *a* = 11.99 Å, *Z* = 2 of *C12A7* contains two molecules. It is characterized with a positively charged lattice framework [Ca$_{24}$Al$_{28}$O$_{64}$]$^{4+}$+2O^{2-} having

---

* Corresponding author: Pantelija.Nikolic@sanu.ac.yu

12 crystallographic cages per unit cell. The crystal structure of *C12A7* is shown in Fig. 1a viewed from the [111] direction where the unit cell is indicated with a black frame. Fig. 1b gives the structure of a cage where an O^{2-} anion is accommodated to compensate the positively charged framework and is coordinated with six Ca^{2+} cations which makes a cage wall. This transparent insulating oxide can also be converted into an electrical conductor [2]. ESA spectra of *C12A7* samples prepared in different conditions were measured in [3].

Fig. 1 a) The crystal structure of *C12A7* viewed from [111] axes where the unit cell includes two molecules and twelve cages having a free space; b) The structure of a cage where six Ca^{2+} ions coordinate to the center of the cage.

In this work thermal diffusivity, optical absorption and some electronic transport properties were investigated for *C12A7* samples before and after hydrogen and ultraviolet optical treatment using a photoacoustic method.

2. Experimental Results

In order to obtain sintered $12CaO \cdot 7Al_2O_3$ powders of $CaCO_3$ and Al_2O_3 were used. They were milled for 120 minutes in a mill. Then the obtained powder was pressed into disks of approximately 10 mm in diameter with the pressure of 1000 kg/cm^2. The discs were then sintered at 1300ºC for 30, 120 and 240 minutes. X-ray analysis of the obtained samples confirmed that during reactive sintering the compound $12CaO \cdot 7Al_2O_3$ (*C12A7*) was obtained.

Photoacoustic phase and amplitude spectra of *C12A7* sintered pellets were measured using a photoacoustic cell protected against surrounding influences as described elsewhere [4]. The photoacoustic phase and amplitude signals were measured employing the experimental arrangement, given in Fig. 2.
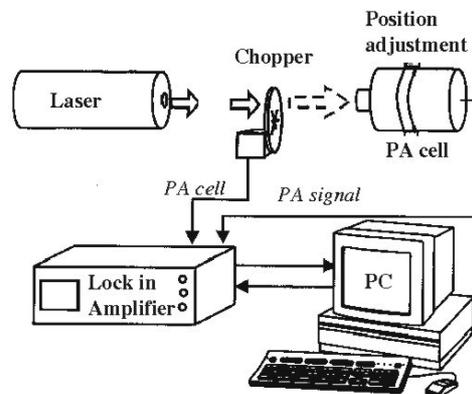

Fig. 2 The experimental set-up for photoacoustic measurements.

A He-Cd 10 mW laser was used as the optical source, which was modulated with a mechanical chopper. The sample was mounted directly on the front side of the electret microphone, which had a 3 mm diameter circular window as the sound inlet. One side of the sample surface was always highly polished, while the opposite side was rougher having been polished with abrasive silicium carbide P1000 sandpaper. A photoacoustic phase diagram versus the modulation frequency, when the highly polished side of the sample was in contact with the electret microphone and the rough side was illuminated, is given in Fig. 3a for a typical *C12A7* sample 340 μm thick, which was not treated with either hydrogen or UV light. A similar PA phase signal versus the modulation frequency, in the case when the rougher side of the sample was in contact with the electret microphone and the highly polished side was illuminated is given in Fig. 3b. The amplitude spectra versus the modulation frequency, for the same samples when the highly polished side of the sample was in contact with the microphone or vice versa, are given in Fig. 3c and Fig. 3d, respectively. It is obvious, comparing Figs. 3a, c with Figs. 3b,d that PA signals are bigger when the examining surface is better polished.
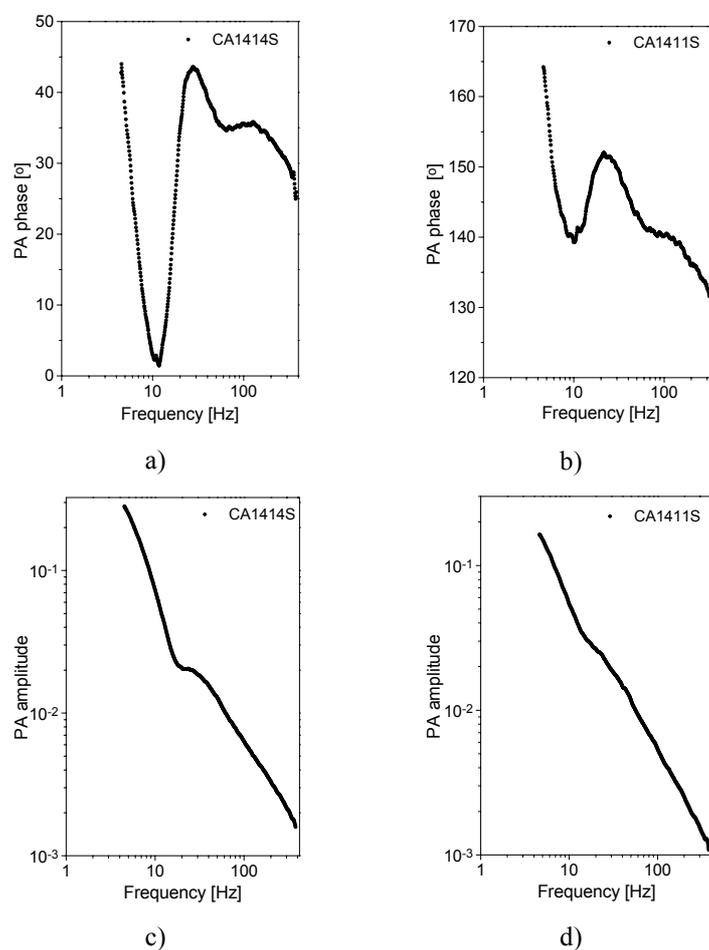

a)

b)

c)

d)

Fig. 3 Photoacoustic phase (a, b) and amplitude (c, d) diagrams for a typical *C12A7* sample 340 μm thick, respectively. In Figs. 3a,c the highly polished side of the sample is in contact with the electret microphone. In Figs. 3b,d the rough side is in contact with the electret microphone.

In Fig. 4 the phase (a) and amplitude (b) PA signals versus the modulating frequency are represented for three different samples: CAA4H1S (590 μm thick and sintered in air for 240 minutes), CA111AS (670 μm thick and sintered in air for 120 minutes) and CAF1S

(sample 730 µm thick sintered first in air and then in hydrogen atmosphere and finally exposed to ultraviolet light).
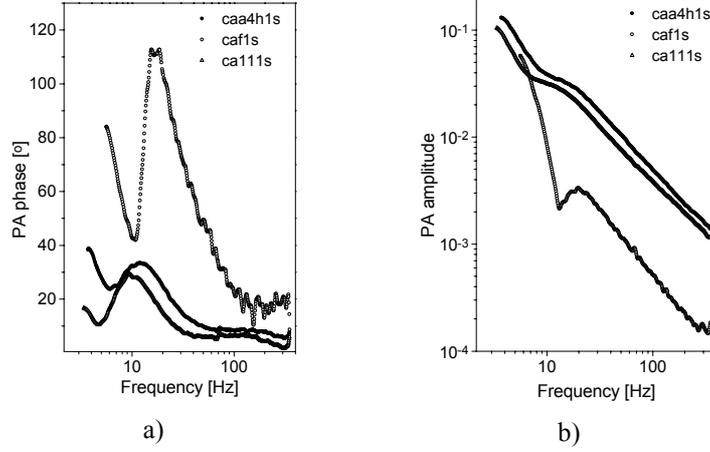

a)   b)

Fig. 4 The phase (a) and amplitude (b) PA diagrams versus the modulating frequencies for three different *C12A7* sample (590 µm and 670 µm thick sintered in air for 240 minutes and 120 minutes, respectively, and sample 730 µm thick sintered first in air and then in hydrogen atmosphere and then exposed to UV light).

3. Discussion

The theoretical explanation and analysis of experimental results are based on the thermal piston model of Rosencwaig and Gersho [5], where the PA signal is due to periodic temperature variations on the bounding sample-backing (air) surface, which can be expressed using the following equation:

$$\delta P(\omega) = \gamma \frac{P_0 \theta_s}{T_0 l_b \sigma_g}, \tag{1}$$

where P_0 and T_0 are the ambient pressure and temperature (room temperature), l_b is the distance between the sample and the microphone membrane, σ_g is a complex thermal diffusion coefficient of backing and γ is the adiabatic constant. The sample's temperature fluctuations at the sample-backing interface, θ_s, is an essential feature, which should be obtained. Several one-dimensional theoretical approximate models exist [6-7] which can be used to determine thermal and electronic transport properties in a heat transmition configuration. Non-adiabatic (isochoric) contributions to pressure generations can be neglected because the gas-length (l_b) is much larger compared with its thermal diffusion length (μ_g) and the sample is not transparent ($al \gg 1$). Korpiun and Büchuer [8] assumed that pressure fluctuations in a gas chamber of the PA cell is an isochoric process not an isobaric-adiabatic process. In our case, for the cylindrically shaped PA configurations, the gas chamber, V_b, is the microphone chamber V_m. For the used electret microphone, the gas length, l_b, and its diameter are much smaller compared with the sound wavelength. For the modulation frequency $f = 1$ kHz the sound wavelength in air is about 34 cm while the gas length is about 1 mm. The pressure fluctuation in the PA cell may then be considered to be of constant amplitude over the entire volume. Following the explanation of Korpiun and Büchuer [8] the relation for the pressure fluctuation in the microphone chamber can be given:

$$\delta P(\omega) = \frac{P_0}{T_0} \frac{V_s}{V_m} \delta T(\omega) = \frac{P_0}{T_0} \left(\frac{R_s}{R_m}\right)^2 \frac{1 - e^{-k_b l_b}}{k_b l_b} \theta_s(l_S, \omega), \tag{2}$$

where $V_s = A_s l_b$ and $A_s = R_s^2$ is the surface of the inlet window, $V_m = R_m^2$ and R_m is the radius of the microphone chamber. This relation shows that for $l_b \to 0$ the pressure fluctuations vanish. If l_b increases, the pressure fluctuation reaches its maximum when l_b is approximately equal to the thermal diffusion length, μ_g. For the case of thermally thick gas ($l_b >> \mu_g$):

$$\delta P(\omega) = \frac{P_0}{T_0} \left(\frac{R_s}{R_m}\right)^2 \frac{1}{k_b l_b} \theta_s(\omega) \cong \frac{1}{l_b}, \tag{3}$$

which is practically the relation predicted from the Rosencwaig and Gersho model (RG) [5]. A multiple $\gamma = C_p/C_v$ exists. The heat flow from the sample to the gas leads to a change in the internal energy $\overline{U}$ of the gas at constant volume. The relationship between the internal energy and pressure change, for an isochoric process is:

$$\delta U = \frac{\rho_b C_v V_m}{\beta_T B} \delta P, \tag{4}$$

where C_v is the (gas) specific heat at constant volume, ρ_b is the mass density of gas, β_T is the volume thermal expansion coefficient and B is the bulk modulus. In the case of an average temperature fluctuation in the gas, $\delta T(w)$, the mean change of the gas internal energy is:

$$\delta \overline{U} = \rho_b C_v V_s \delta T(\omega), \tag{5}$$

where

$$\delta T = \frac{1}{l_b} \int_l^{l+l_b} \theta_b(x, \omega) dx, \tag{6}$$

where $\theta_b(x, w)$ is the full solution of the thermal diffusion equation in the backing (gas).

$$\left(\frac{d^2}{dx^2} - \sigma_i^2\right) \theta_i(x) = 0 \quad i = g, b, \tag{7a}$$

$$\left(\frac{d^2}{dx^2} - \sigma_s^2\right) \theta_s(x) = Q(x), \tag{7b}$$

where $\theta_i(x)$ is periodic part of the temperature in the PA cell, $\sigma_i^2 = j\omega/D_{Ti}$, D_{Ti} is the thermal diffusivity of layer i (s, g and b denote sample, gas and backing, respectively). $\theta(x)$ represents the thermal source at point x of the sample. Finally, $\Phi_s(-l, \omega)$ is the temperature variation of the sample surface which is in contact with the electret microphone, solving the system of two coupled diffusion equations as described elsewhere [9]. Thus the PA signal can, finally, be calculated using the following equation:

$$S = C_{td}(\Phi^T(-l) + \Phi^{BR}(-l) + \Phi^{SR}(-l)), \tag{8}$$

where $C_{td} = g_0 P_0 / T_0 k_b l_b$ and it represents the factor of thermodiffusion. $\Phi^T(-l)$, $\Phi^{BR}(-l)$ and $\Phi^{SR}(-l)$ are components of the periodic temperature related to the rear surface of the sample and they are the thermalization (T), bulk (BR) and surface (SR) recombination components of the temperature distribution, respectively. In our case the thermalization component $\Phi^T(-l)$ is dominant. This happens at low modulation frequency when the sample thickness l is smaller

than the thermal diffusion length μ_b ($\mu_b = (D_T / \pi f)^{1/2}$). The sample behaves as thermally thin when $\mu_b > l$ because at higher modulation frequencies μ_b decreases and the sample behaves as thermally thick. Then the effect of $\Phi^{BR}(-l)$ and $\Phi^{SR}(-l)$ increases and cannot be neglected.

The experimental phase and amplitude PA diagrams were compared with theoretically calculated diagrams using the previously proposed model. The values of thermal and transport parameters were obtained using the best square fitting procedure. A fitting program was developed that enables the user to choose the values of parameters in the mathematical model. Practically, all of the parameters used can be fitted. The user selects the magnitude of the change of each parameter. If some parameter should stay unaltered then the change of the parameter should be selected to be zero. One can, simultaneously, fit the phase and amplitude separately or both together. The fitting error can be estimated using one of the following criteria: (a) the sum of absolute differences between the calculated and experimental values; (b) the sum of the squares of differences between the calculated and the experimental values; (c) the sum of relative errors; (d) the sum of the squares of the relative errors.

Therefore, the experimental curve can be compared with the theoretical one obtained for the given parameters from the mathematical model. Their values can be determined during the fitting procedure. In this way, the user can follow the change of the errors and see whether the fitting procedure converges or not. Depending on this, the user can react (or not) in the following way: (a) to continue the fitting procedure, if the error is continuing to decrease *or* (b) to change the values of some parameters if the decrease of the error is extremely small (or if it does not change). A typical example of this fitting procedure of phase and amplitude diagram is shown in Fig. 5a and Fig. 5b, respectively, for a *C12A7* sample, 590μm thick and sintered in air for 240 minutes. The full line represents the theoretical curve while the experimental values are given with dots. It is obvious that the phase diagram was better fitted while the amplitude fitted diagram differs from experimental at low frequency (below 10 Hz) because of the decrease of microphone sensitivity in that range.
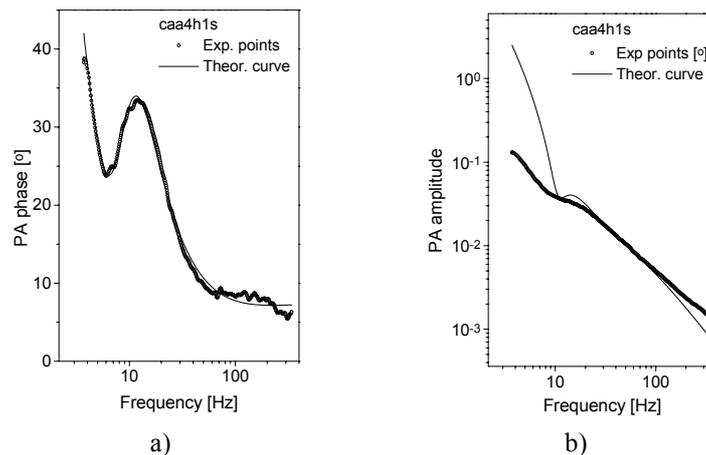

a)   b)

Fig. 5 The phase and amplitude PA diagrams for a *C12A7* sample 590 μm thick. The full line represents the theoretical curve while the experimental values are given with dots.

Tab. I contains the values of the fitted parameters obtained by the fitting procedure for six PA spectra. Three spectra are for the samples sintered only in air for 30, 120 and 240 minutes. The other three spectra were measured for samples additionally sintered in hydrogen atmosphere for one hour at 700ºC and then exposed to an ultraviolet light beam.

Tab. I Numerically determined parameters for $12CaO \cdot 7Al_2O_3$ samples sintered in the air and hydrogen atmosphere for different time.

Sample	CATT2S	CA111AS	CAA4H1S	CAC602S	CAD129S	CAF1S
Atmosphere	Air	Air	Air	H_2 and UV	H_2 and UV	H_2 and UV
Time [min]	30	120	240	60	120	240
D_T [m^2/s]	$0.15 \cdot 10^{-6}$	$0.17 \cdot 10^{-6}$	$0.19 \cdot 10^{-6}$	$0.42 \cdot 10^{-6}$	$0.4 \cdot 10^{-6}$	$0.29 \cdot 10^{-6}$
D [m^2/s]	$0.46 \cdot 10^{-6}$	$0.3 \cdot 10^{-6}$	$0.3 \cdot 10^{-6}$	$0.55 \cdot 10^{-7}$	$0.6 \cdot 10^{-6}$	$0.30 \cdot 10^{-5}$
α [m^{-1}]	7822	11914	12464	13467	9974	13482
τ [ms]	36	10.5	7.8	4.6	12	1.5
s_b [m/s]	11.1	0.09	0.34	0.27	0.02	0.07
s_g [m/s]	36.5	$0.24 \cdot 10^{-3}$	$0.49 \cdot 10^{-1}$	0.09	0.003	0.03
d [μm]	525	670	550	660	890	730

The thermal diffusivity for the samples sintered in air gradually increases with the time of sintering. For the samples that were afterwards additionally sintered in an atmosphere of hydrogen and then exposed to the light beam of an ultraviolet lamp, the thermal diffusivity was practically twofold. It is shown in Fig. 6. Obviously, one needs more samples sintered at various conditions to be able to get very clear conclusions about the change of thermal and other properties of *C12A7*. But our work can show that the thermal diffusivity of this novel material changes depending on conditions of sample treatment. The PA method can definitely be used for characterization of *C12A7* whose strong emissivity of negative ions O⁻, as well as easy and economical fabrication, may be used in the near future.
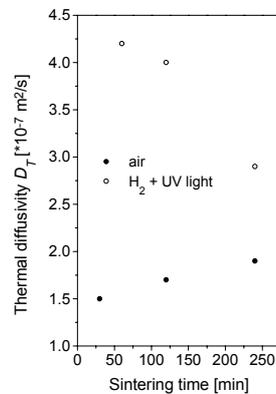

Fig. 6 The thermal diffusivity versus the time of sintering for the samples sintered in air (•) and additionally sintered in hydrogen atmosphere and exposed to the UV beam (o).

Besides thermal diffusivity, Tab. I contains other parameters calculated during the fitting procedure. The diffusion coefficient of free carriers (D) is about $0.3 \cdot 10^{-6}$ m^2/s. That implies a free carrier mobility of about 0.1 cm^2/Vs. For the samples treated in hydrogen atmosphere μ increases and for the sample treated 240 minutes it reaches the value of about 1 cm^2/Vs. The calculated optical absorption coefficient is more stable between 7800 and 13500 m^{-1} for all investigated samples. The excess carrier lifetime τ is between 36 and 7.8 ms for the sample sintered in air. It decreases when the time of sintering increases. Similar properties are noted for samples treated in hydrogen and with ultraviolet light. The recombination velocity tends to be smaller for the samples treated with either hydrogen or UV light.

4. Conclusion

In this work the thermal diffusivity and some other electrical and optical parameters of an interesting material $12CaO \cdot 7Al_2O_3$ (*C12A7*) produced by reactive sintering were investigated using the photoacoustic method. It has been recently proposed that this material could be used like a solid electrolyte as a strong O^- emitter, which is about three orders of magnitude higher than the O^- current density emitted from Y_2O_3-stabilized ZnO_2 (YSZ) electrolyte [1]. We have shown that the thermal diffusivity is about $0.3 \cdot 10^{-6}$ m^2/s for the samples sintered only in air and it increases about twice if the samples are additionally sintered in hydrogen and, finally, exposed to UV light.

We feel that the photoacoustic method can be very useful for characterization of this material during further investigations of the possibility of the production of *C12A7* thin films with a transmission loss of less than 1 % in the visible light range [2], which will be essential in the emerging invisible circuit technology [10].

References

1. Q. X. Li, K. Hayashi, M. Nishioka, H. Kashiwagi, M. Hirano, Y. Torimoto, H. Hosono, M. Sadakata, Appl. Phys. Lett., **80** (22) (2002) 4259-4261.
2. K. Hayashi, S. Matsulshi, T. Kamlya, M. Hirano, H. Hosono, Nature, **419** (2002) 462-465.
3. K. Hayashi, M. Hirano, S. Matsuishi, H. Hosono, J. Am. Chem. Soc., **124** (5) (2002) 738-739.
4. D. M. Todorovic, P. M. Nikolic, Opt. Eng., **36** (1997) 432.
5. A. Rosencwaig, A. Gersho, J. Appl. Phys., **47** (1976) 64.
6. A. N. Vasilev, V. B. Sandomirski, Sov. Phys. Semicond., **18** (1984) 1095.
7. A. Pinto Neto, H. Vargas, N. Leite, L. C. M. Miranda, Phys. Rev. B, **40** (1989-II) 3924.
8. P. Korpiun, B. Büchuer, Appl. Phys. B, **30** (1983) 121.
9. P. M. Nikolic, S. S. Vujatovic, D. M. Todorovic, M. Miletic, A. Golubovic, A. I. Bojicic, F. Kermendi, K. T. Radulovic, J. Elazar, J. Appl. Phys., **36** (1996) 1006.
10. G. Thomas, Nature, **389** (1997) 907.